Electronic Supporting Information

Group 2 metal (Mg, Ca, Sr) silylamides supported by a cyclen-derived macrocyclic polyamine

Debabrata Mukhejee, Satoru Shirase, Klaus Beckerle, Thomas P. Spaniol, Kazushi Mashima, and Jun Okuda*

Institute of Inorganic Chemistry, RWTH Aachen University, Landoltweg 1, 52056 Aachen, Germany
Graduate School of Engineering Science, Osaka University, Toyonaka, Osaka 560–8531, Japan

Table of Contents

1. Spectroscopic characterization of compounds 1-6.

[(L)Sr{N(SiMe$_3$)$_2$}] (1).

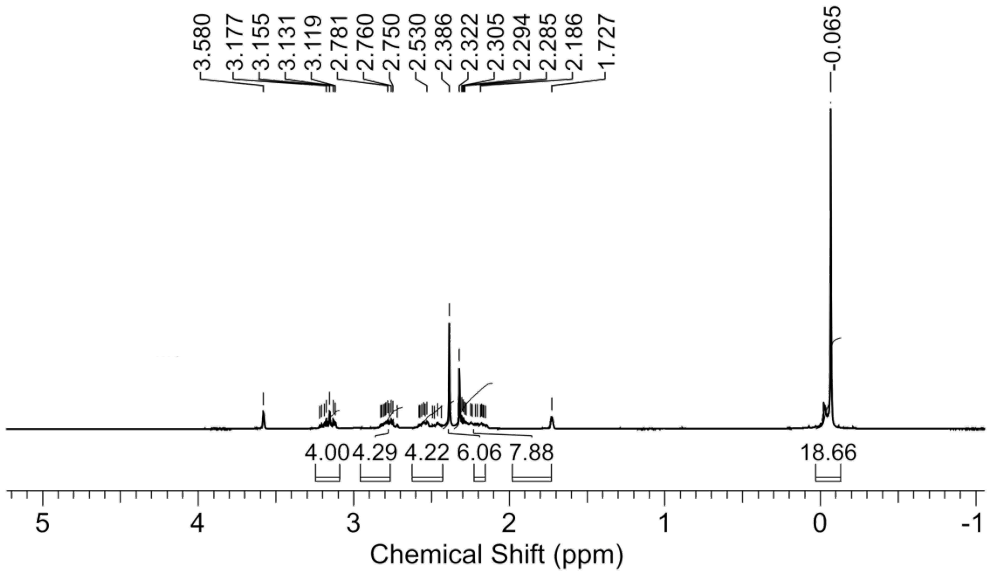

Figure S1. ^{1}H NMR spectrum of **1** in THF-d_8.

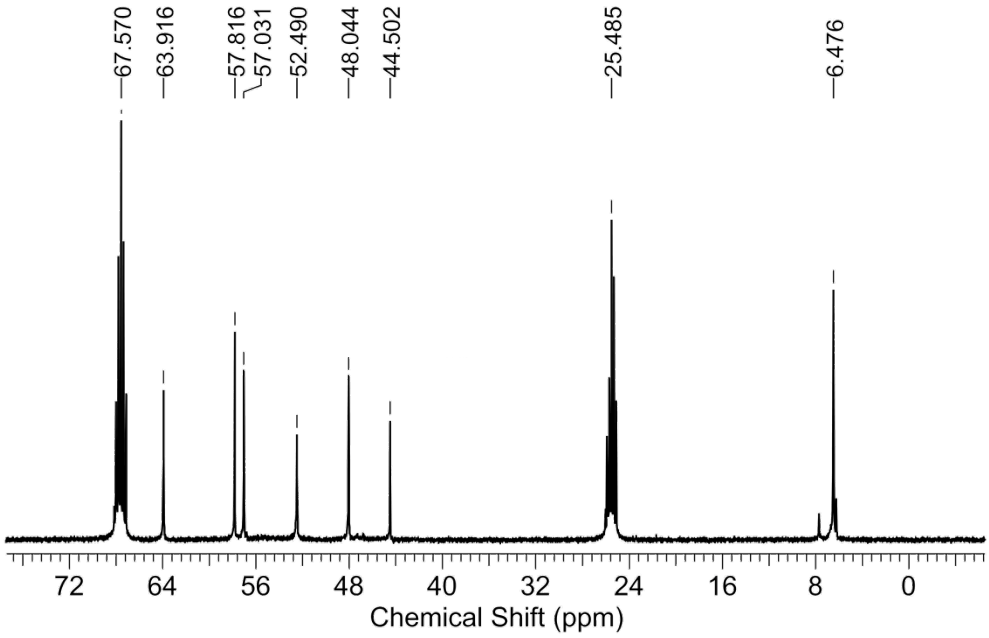

Figure S2. ^{13}C{^{1}H} NMR spectrum of **1** in THF-d_8.

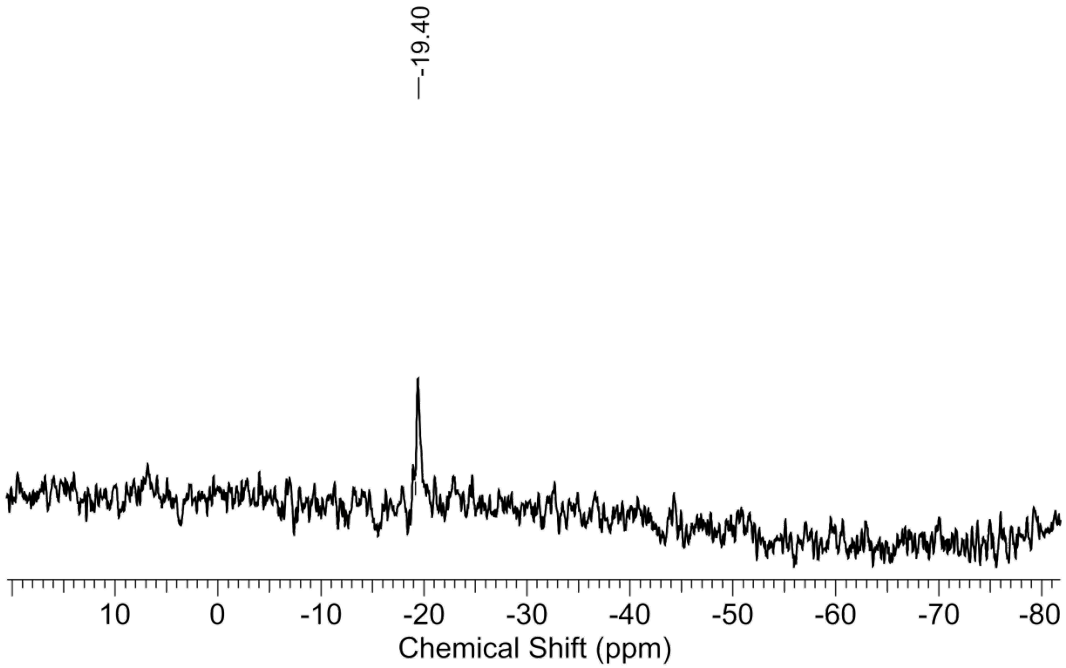

Figure S3. $^{29}Si\{^{1}H\}$ NMR spectrum of **1** in THF-d_8.

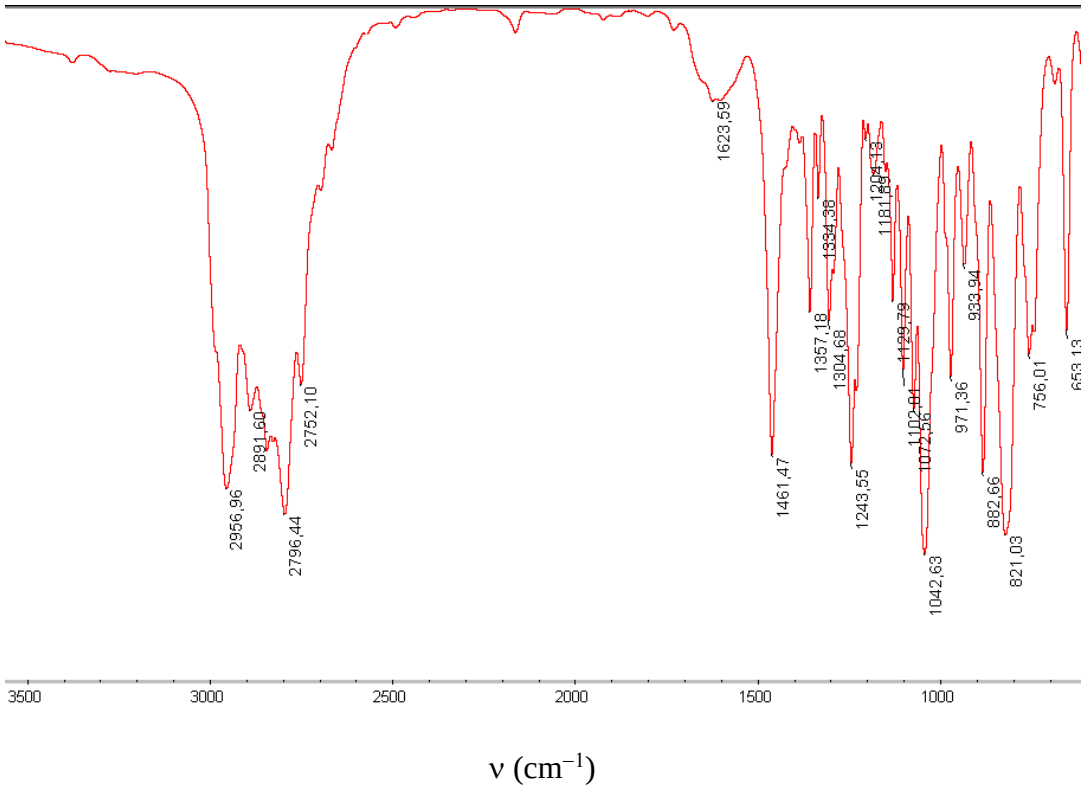

Figure S4. FT-IR (KBr) spectrum of **1**.

[(LH)Sr{N(SiHMe$_2$)$_2$}$_2$] (2).

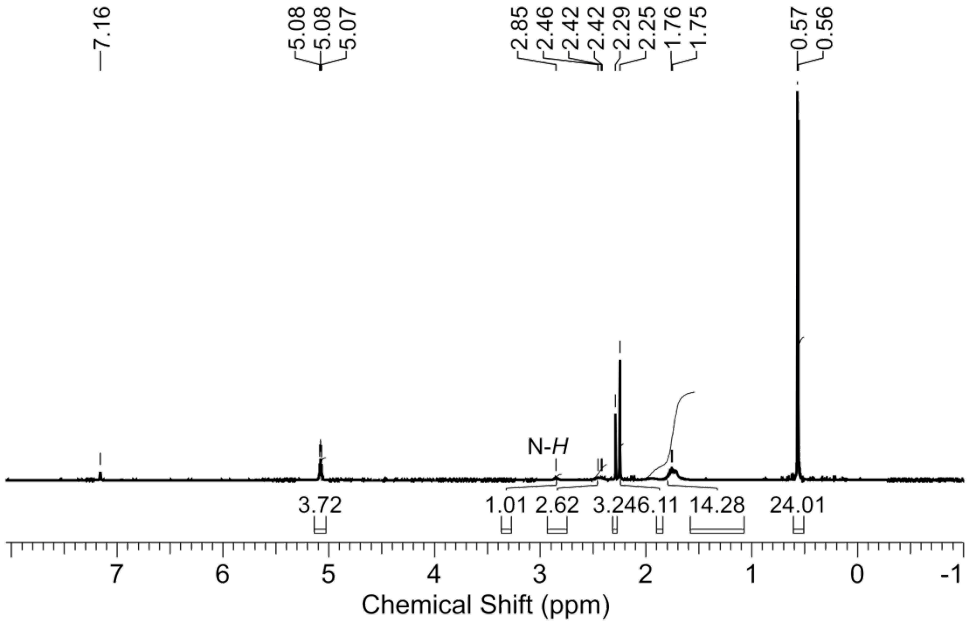

Figure S5. ^{1}H NMR spectrum of **2** in benzene-d_6.

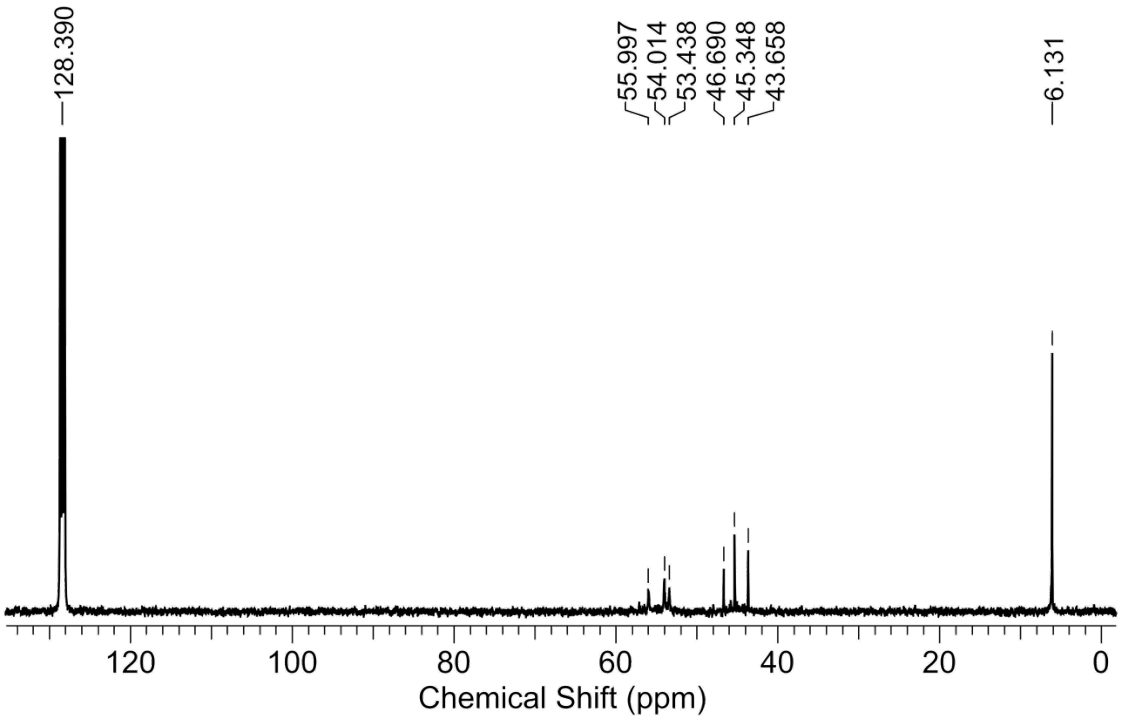

Figure S6. ^{13}C{^{1}H} NMR spectrum of **2** in benzene-d_6.

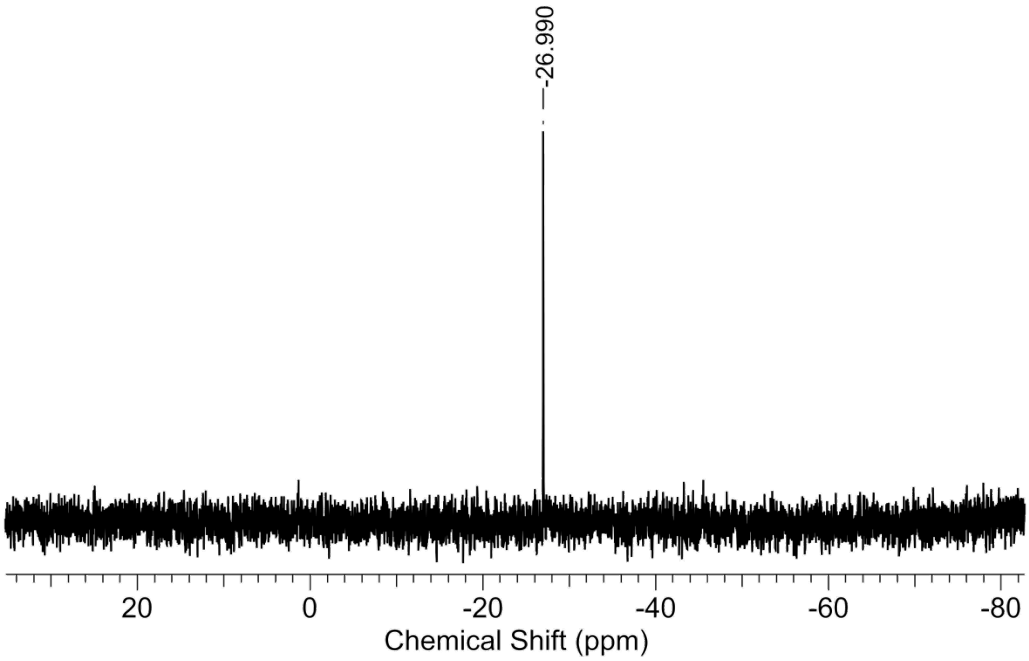

Figure S7. $^{29}Si\{^{1}H\}$ NMR spectrum of **2** in benzene-d_6.

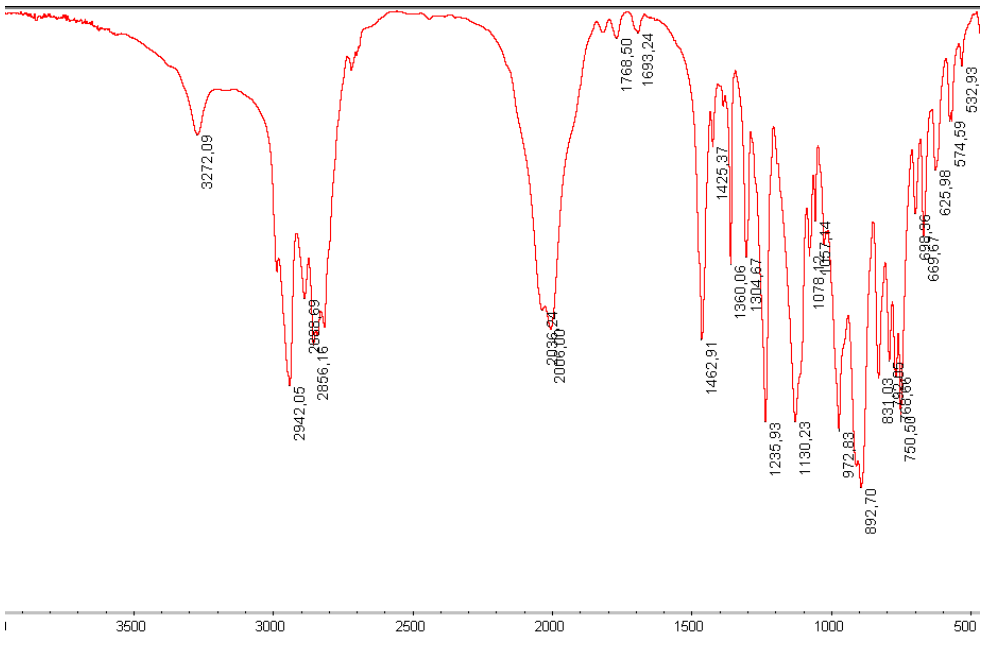

ν (cm^{-1})

Figure S8. FT-IR (KBr) spectrum of **2**.

[{(L)SiMe$_2$N(SiHMe$_2$)}Sr{N(SiHMe$_2$)$_2$}] (3).

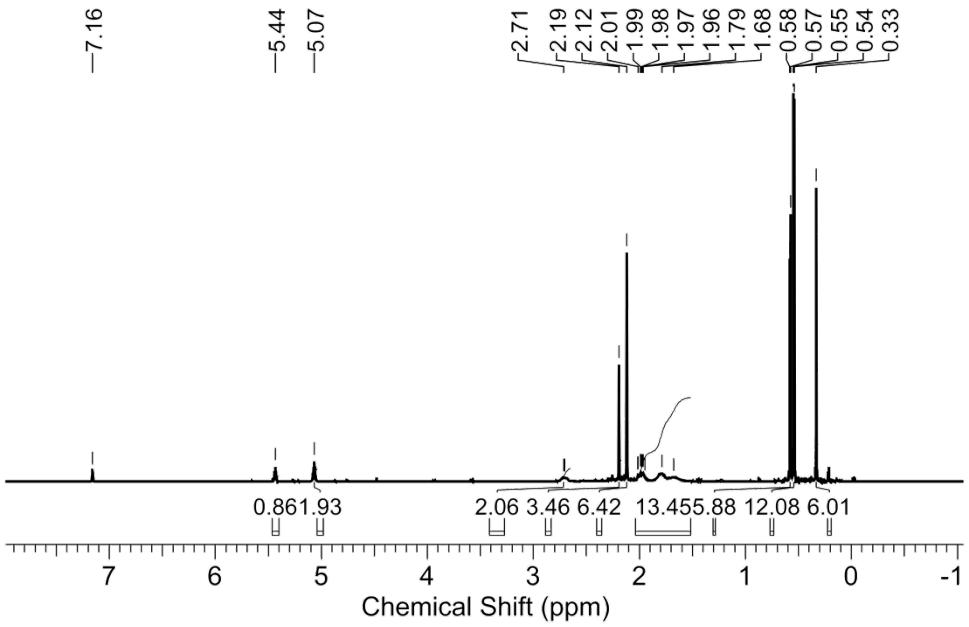

Figure S9. ^{1}H NMR spectrum of **3** in benzene-d_6.

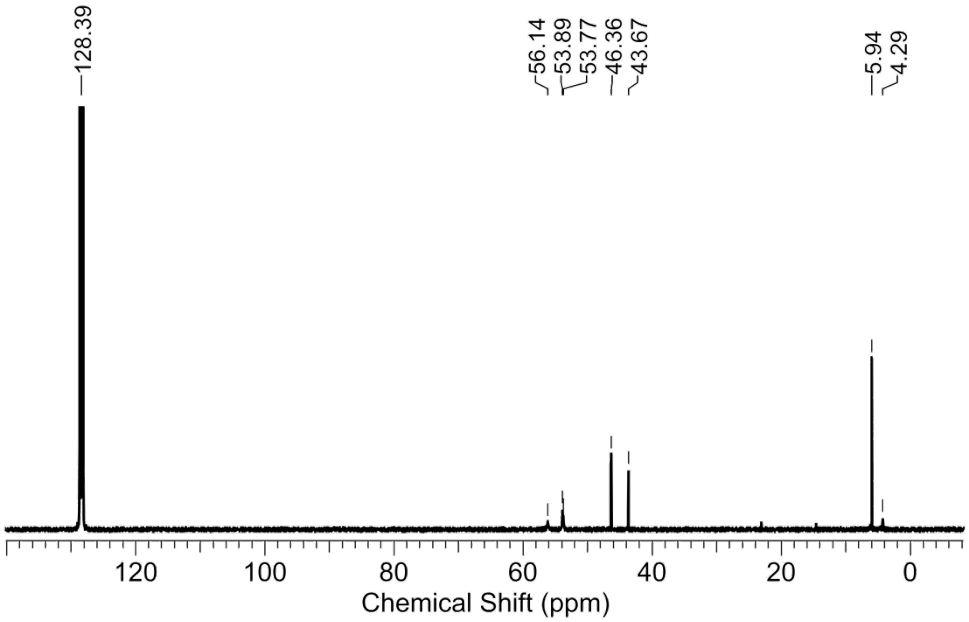

Figure S10. ^{13}C{^{1}H} NMR spectrum of **3** in benzene-d_6.

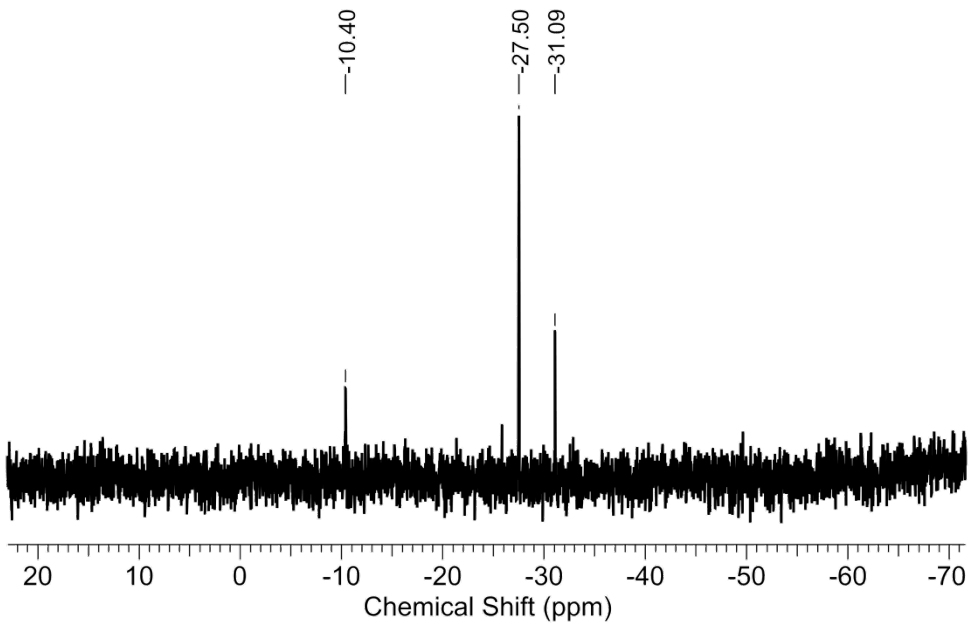

Figure S11. $^{29}Si\{^{1}H\}$ NMR spectrum of **3** in benzene-d_6.

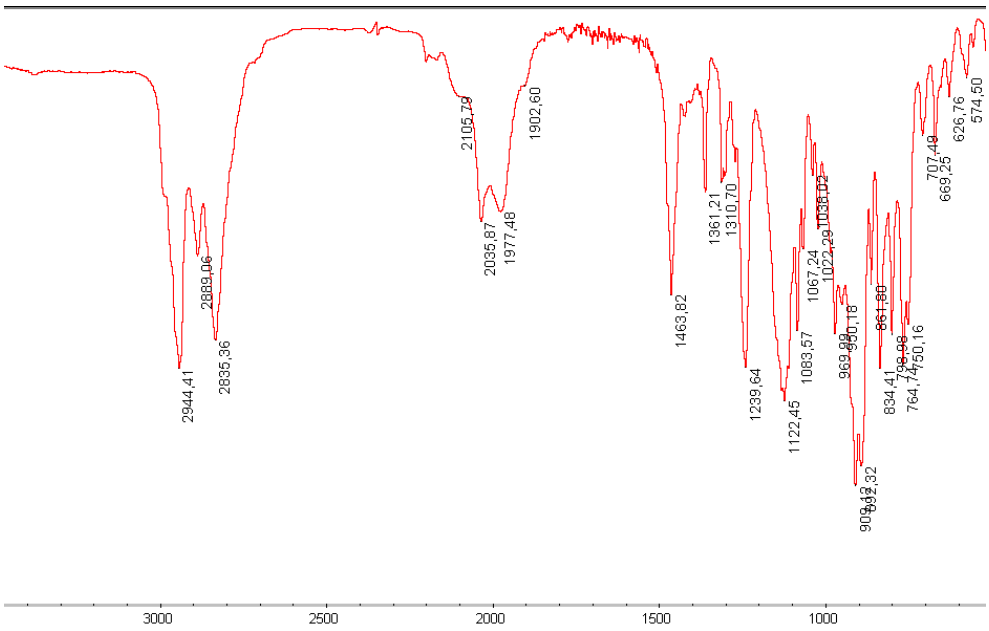

Figure S12. FT-IR (KBr) spectrum of **3**.

[{(L)SiMe$_2$N(SiHMe$_2$)}Sr{N(SiMe$_3$)$_2$}] (4).

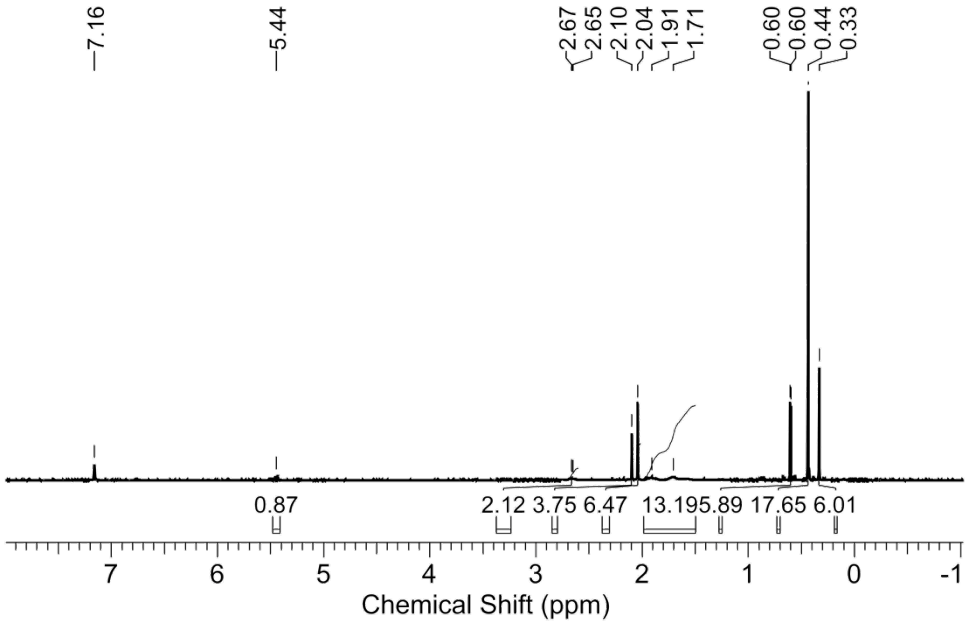

Figure S13. ^{1}H NMR spectrum of **4** in benzene-d_6.

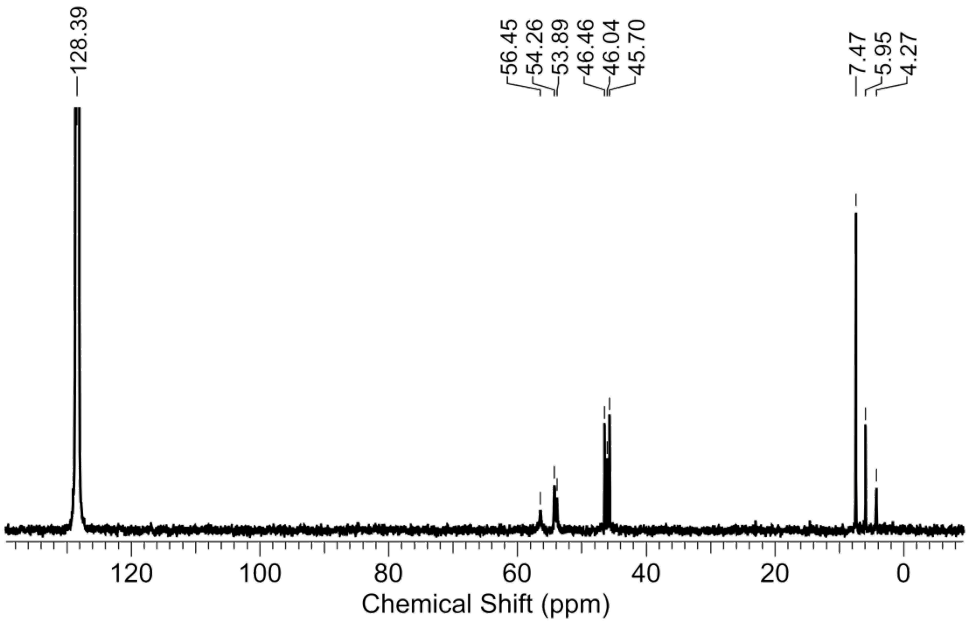

Figure S14. ^{13}C{^{1}H} NMR spectrum of **4** in benzene-d_6.

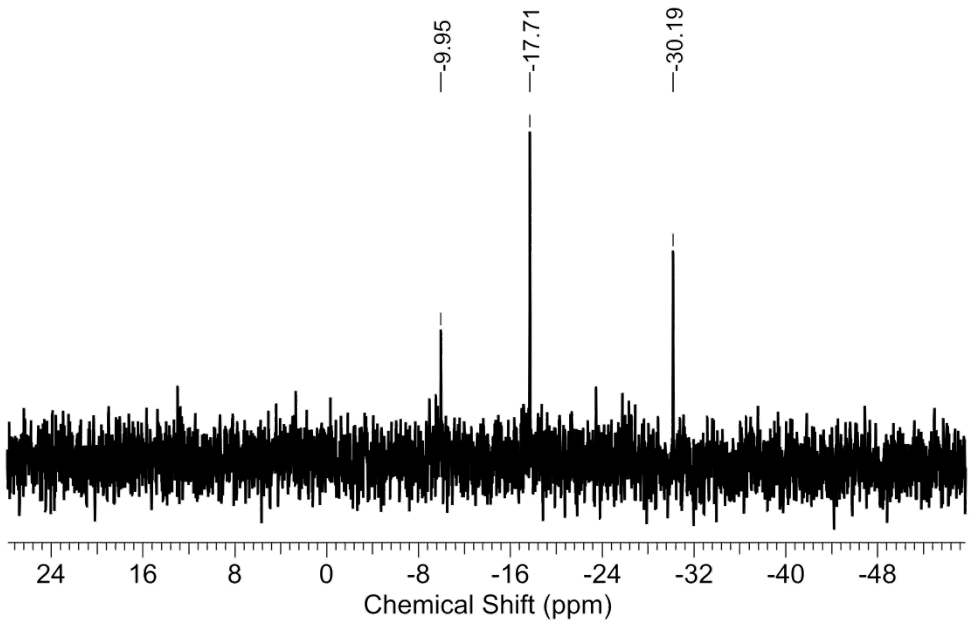

Figure S15. $^{29}Si\{^{1}H\}$ NMR spectrum of **4** in benzene-d_6.

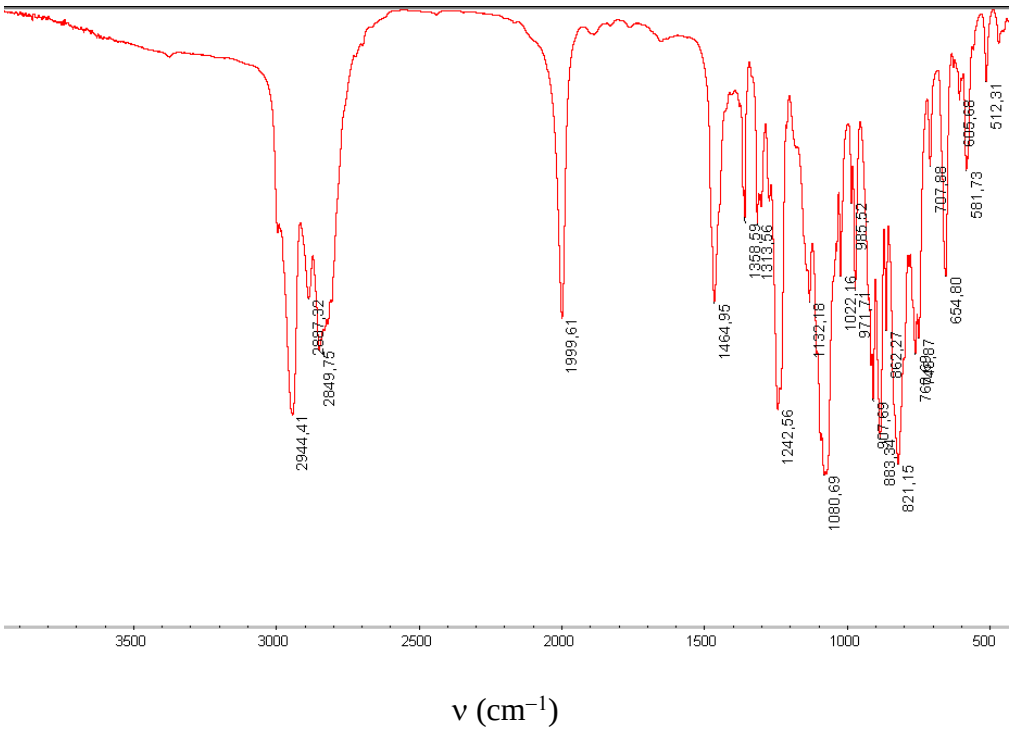

ν (cm^{-1})

Figure S16. FT-IR (KBr) spectrum of **4**.

[(L)Mg{N(SiHMe$_2$)$_2$}] (5).

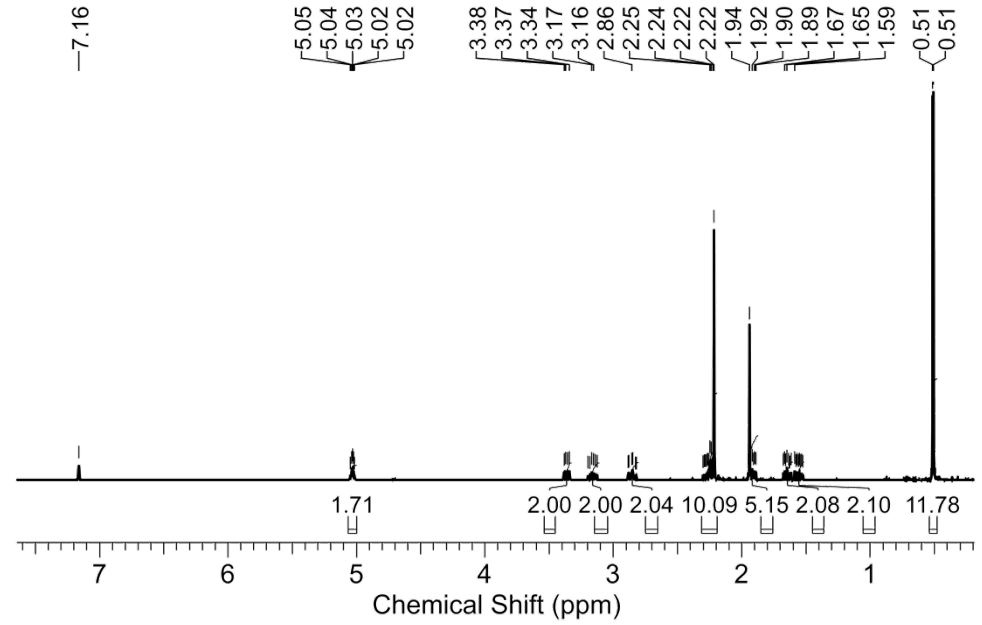

Figure S17. ^{1}H NMR spectrum of **5** in benzene-d_6.

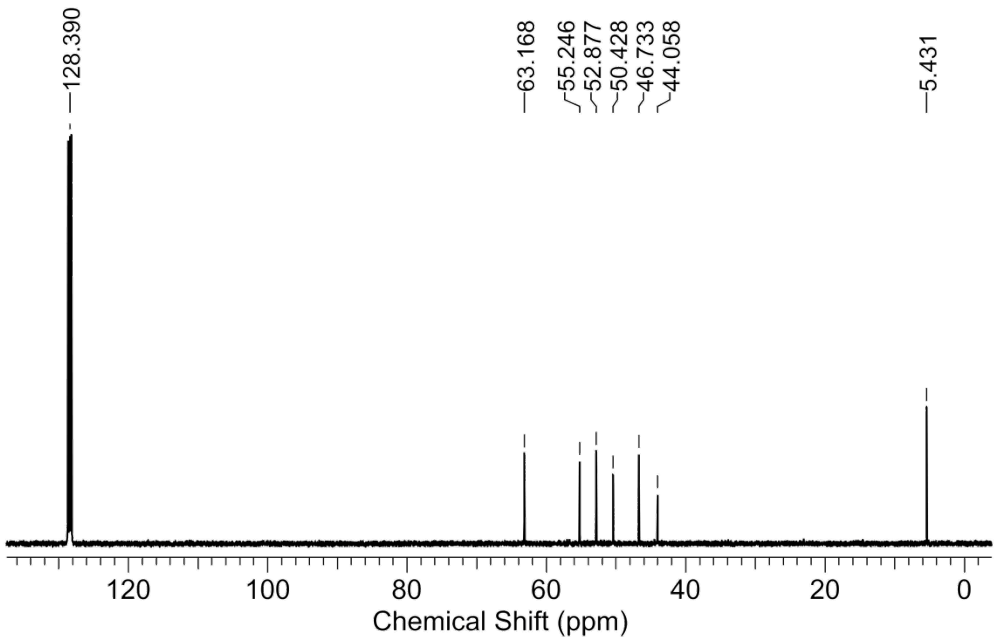

Figure S18. ^{13}C{^{1}H} NMR spectrum of **5** in benzene-d_6.

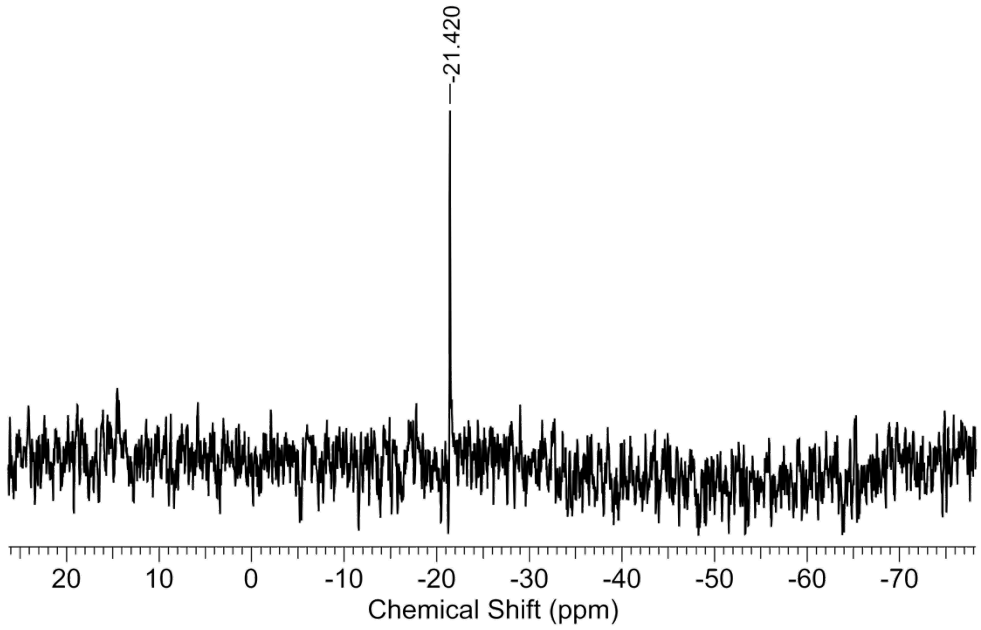

Figure S19. $^{29}Si\{^{1}H\}$ NMR spectrum of **5** in benzene-d_6.

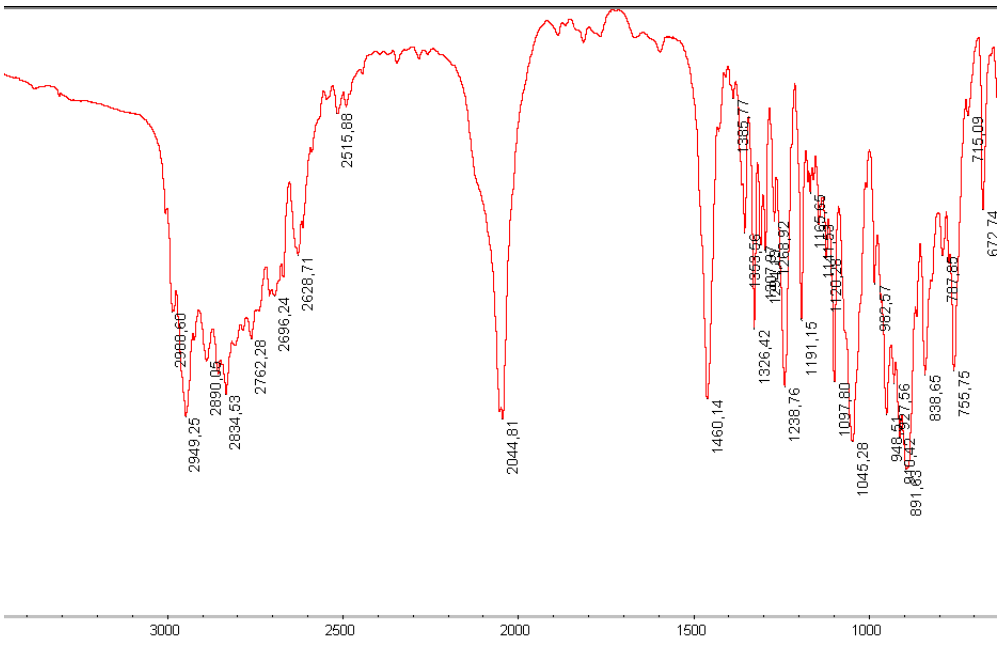

ν (cm^{-1})

Figure S20. FT-IR (KBr) spectrum of **5**.

[(L)Ca{N(SiHMe$_2$)$_2$}] (6).

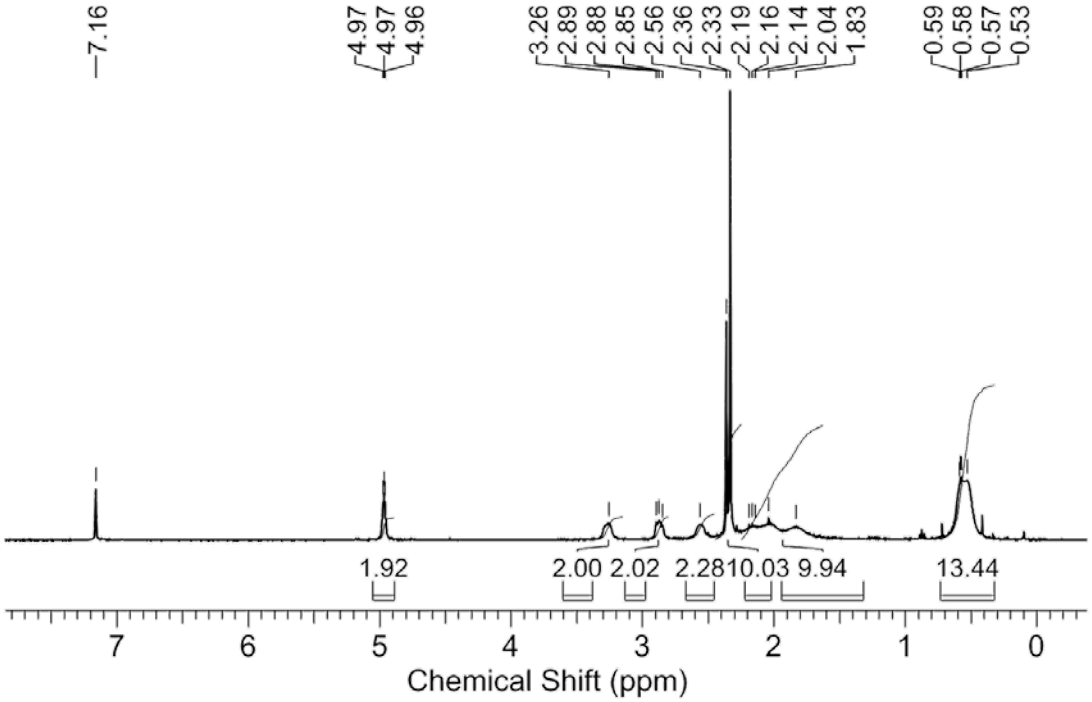

Figure S21. ^{1}H NMR spectrum of **6** in benzene-d_6.

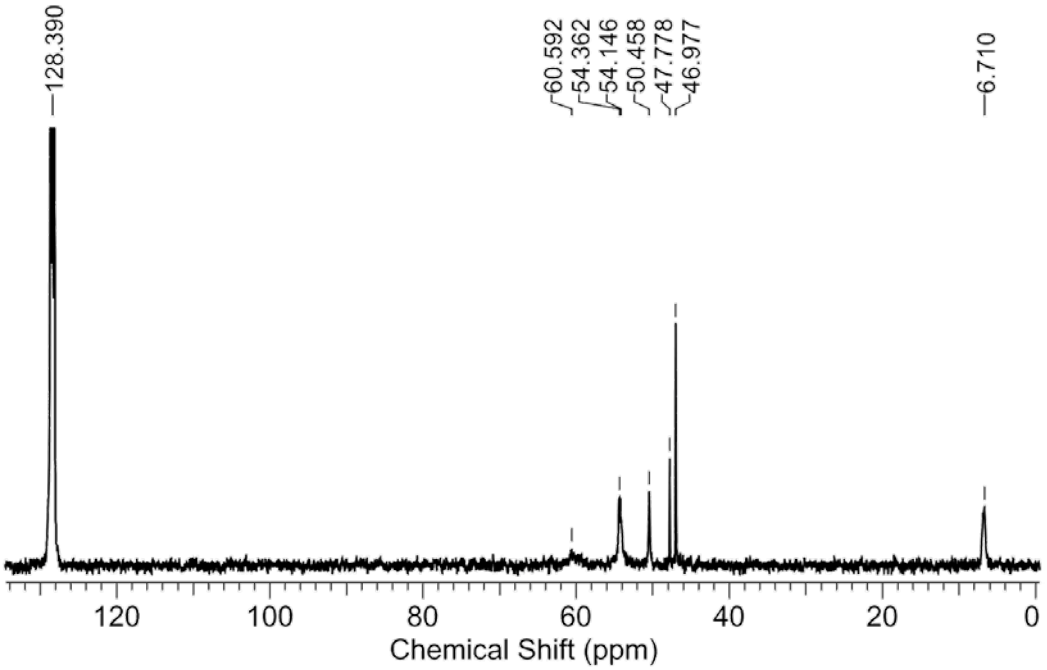

Figure S22. ^{13}C{^{1}H} NMR spectrum of **6** in benzene-d_6.

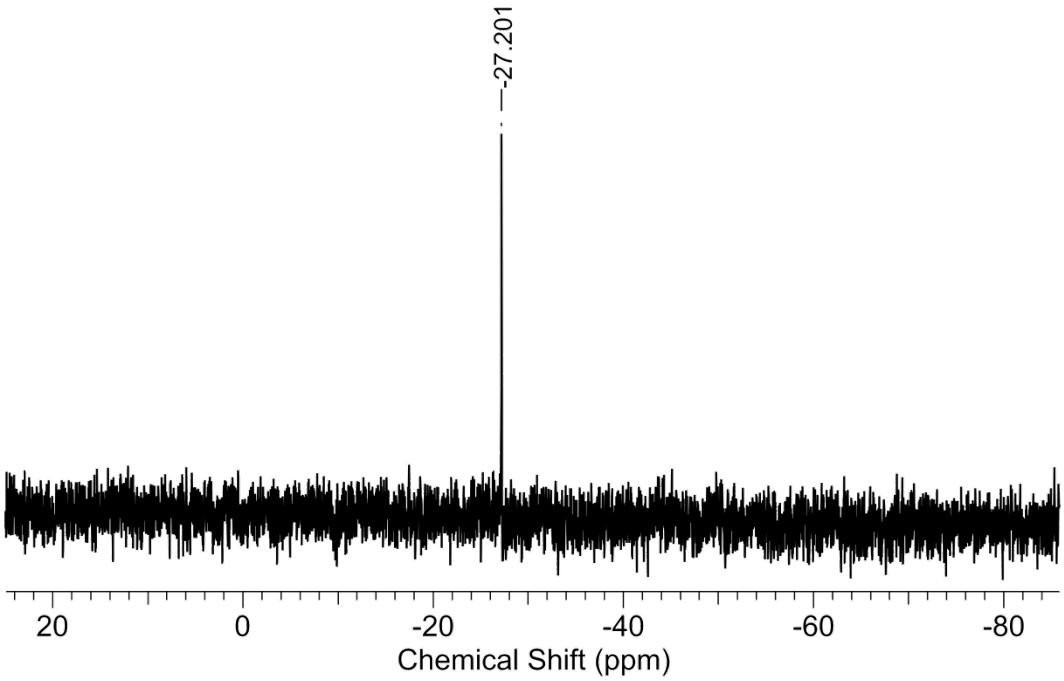

Figure S23. $^{29}Si\{^{1}H\}$ NMR spectrum of **6** in benzene-d_6.

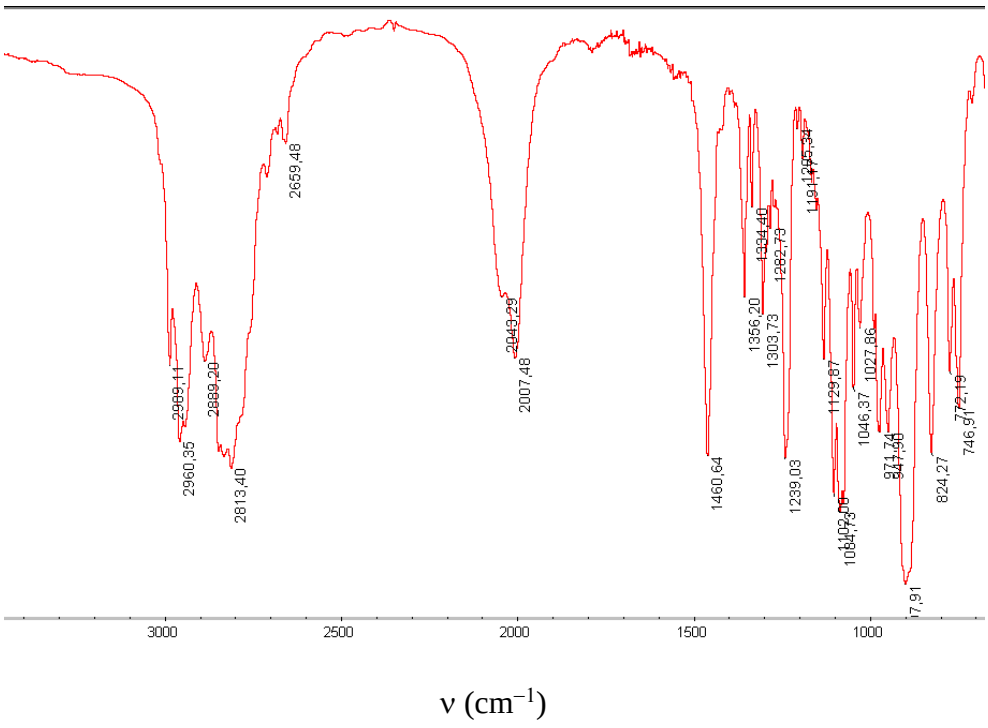

ν (cm^{-1})

Figure S24. FT-IR (KBr) spectrum of **6**.

2. Variable temperature ^{1}H NMR spectroscopy of 6.

Variable temperature NMR analysis was conducted on a freshly prepared toluene-d_8 solution of **6**. The Si*H* resonance at 4.88 ppm ($^1J_{SiH}$ = 164 Hz) at 298 K broadens and shifts downfield at 253 K. Further cooling gives two separate and well-resolved resonances of equal intensity at 5.15 ppm ($^1J_{SiH}$ = 172 Hz) and 4.90 ppm ($^1J_{SiH}$ = 158 Hz) at 193 K with a frequency difference of $\Delta\nu_C$ = 101 Hz. Likewise, the initially broad SiH*Me*$_2$ signal at room temperature splits into four separate resonances at 193 K. For the ligand L, the two sharp N*Me* singlets are severely broadened at low temperature. The C*H*$_2$ protons of the Me$_3$TACD ligand that were initially broad at room temperature become sharper at low temperature with two sets significantly moved to higher field.

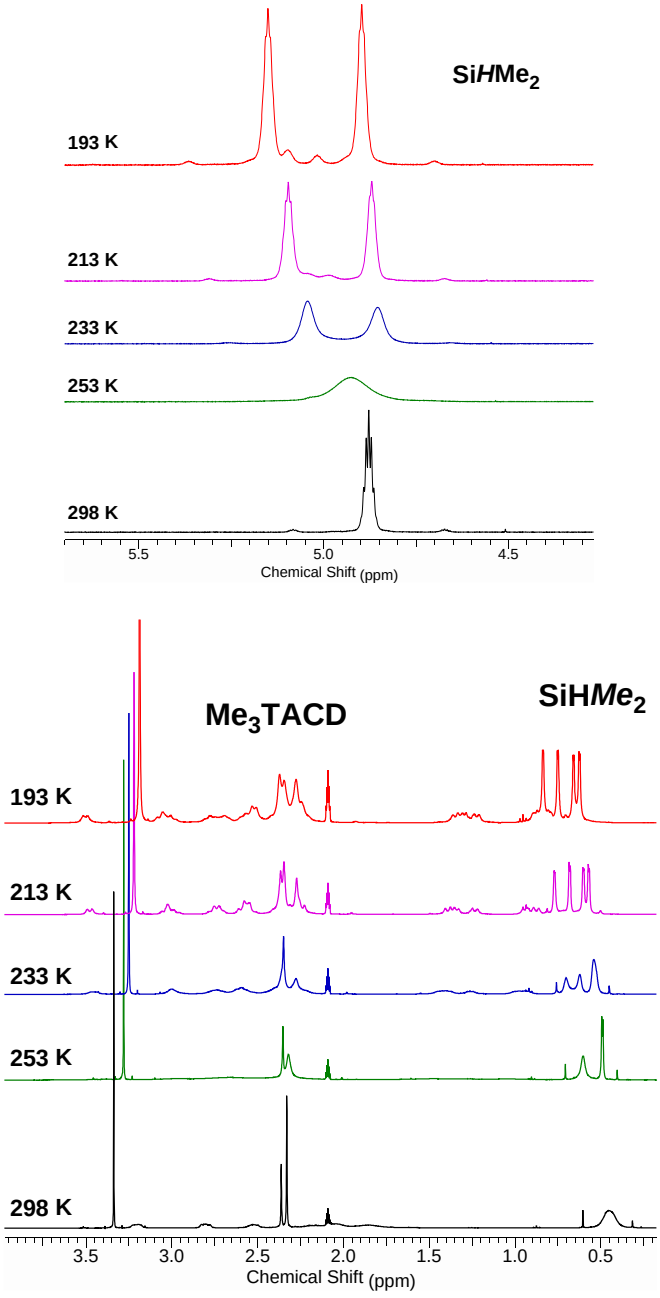

Figure S25. Variable temperature NMR spectra of **6** in Toluene-d_8. **Top:** Si*H*Me$_2$ region. **Bottom:** Me$_3$TACD and SiH*Me*$_2$ region.

3. Line shape analysis and Eyring plot.

Line shape analysis was carried out with the program TopSpin 3.2 starting from a model of two spins-1/2 at 5.10 ppm (experimental low temperature limit) and 4.85 ppm.[S1] An interaction with two further spins with a pseudospin of 3 (each) at 0.58 and 0.79 ppm due to the methyl groups was simulated with coupling constants of J = 4.0 Hz. The reaction was defined as an exchange of spin 1 against spin 2 (and vice versa). The exchange rate and the overall shift of the signals were adjusted manually to obtain the best overlap. This model agrees with a process in which the two silicon-bonded protons exchange at elevated temperature. However, it does not describe the more complex behavior observed for the methyl groups. The significant overall shift of the Si*H*-signals with increasing temperature implies additional processes other than the exchange of β-agostic interactions.

Spin 1 5.1059ppm/pseudospin 0.5
Spin 2 4.8528 ppm/pseudospin 0.5
Spin 3 0.583 ppm/pseudospin 3
Spin 4 0.7929ppm/pseudospin 3
J1/3 4.0Hz
J2/4 4.0Hz
LB 5 Hz
Exchanges
1-2
2-1
k= 0 Hz
Best Overlap
76.398 %
Intensity 40 600

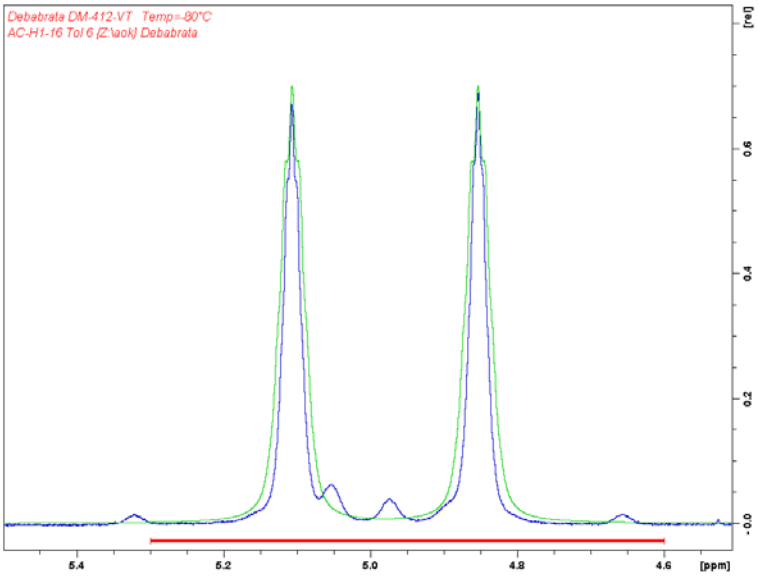

Spin 1 5.06 ppm/pseudospin 0.5
Spin 2 4.81 ppm/pseudospin 0.5
Spin 3 0.583 ppm/pseudospin 3
Spin 4 0.7929ppm/pseudospin 3
J1/3 4.0Hz
J2/4 4.0Hz
LB3.2 Hz
Exchanges
1-2
2-1
k= 9 Hz
Best Overlap
63.744%
Fit 4.6 – 5.4
Intensity 40 550

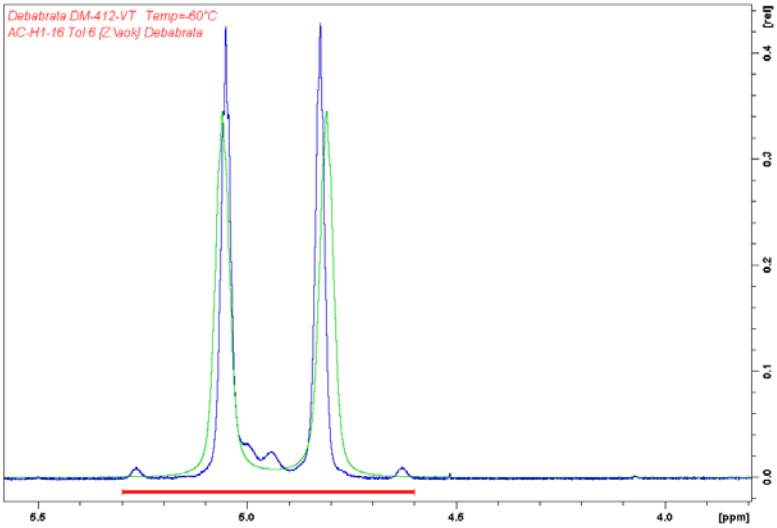

Spin 1 5.0012 ppm/pseudospin 0.5
Spin 2 4.8064 ppm/pseudospin 0.5
Spin 3 0.583 ppm/pseudospin 3
Spin 4 0.7929ppm/pseudospin 3
J1/3 4.0Hz
J2/4 4.0Hz
LB3.5 Hz
Exchanges
1-2
2-1
k= 31.15 Hz
Best Overlap
81.414%
Fit 4.6 – 5.4
Intensity 40 550

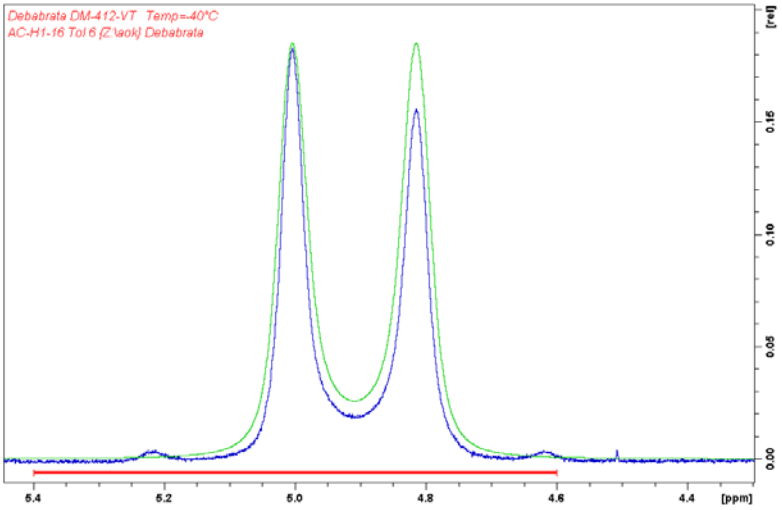

Spin 1 5.0 ppm/pseudospin 0.5
Spin 2 4.75 ppm/pseudospin 0.5
Spin 3 0.583 ppm/pseudospin 3
Spin 4 0.7929ppm/pseudospin 3
J1/3 4.0Hz
J2/4 4.0Hz
LB2.8 Hz
Exchanges
1-2
2-1
k= 552.585 Hz
Best Overlap
92.434%
Fit 4.6 – 5.4
Intensity 24 200

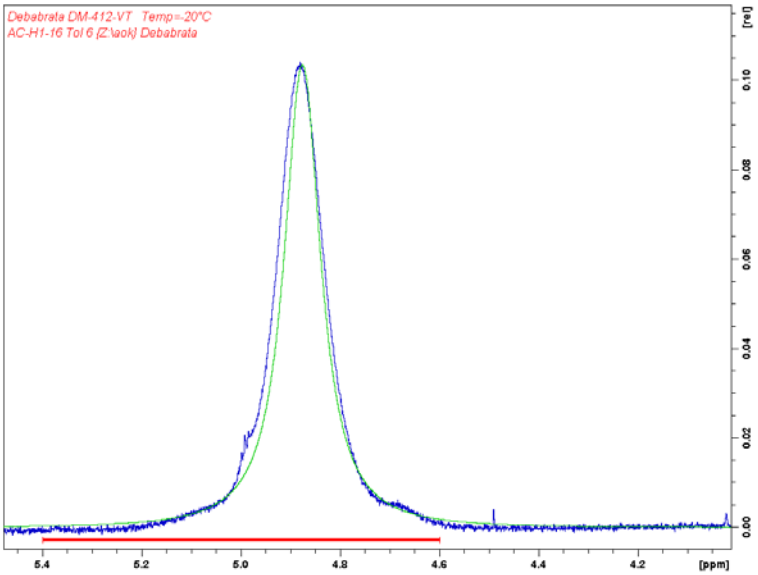

Spin 1 4.955 ppm/pseudospin 0.5
Spin 2 4.705 ppm/pseudospin 0.5
Spin 3 0.583 ppm/pseudospin 3
Spin 4 0.7929ppm/pseudospin 3
J1/3 4.0Hz
J2/4 4.0Hz
LB1.5 Hz
Exchanges
1-2
2-1
k= 10000 Hz
Best Overlap
85.394%
Fit 4.6 – 5.4
Intensity 30 860

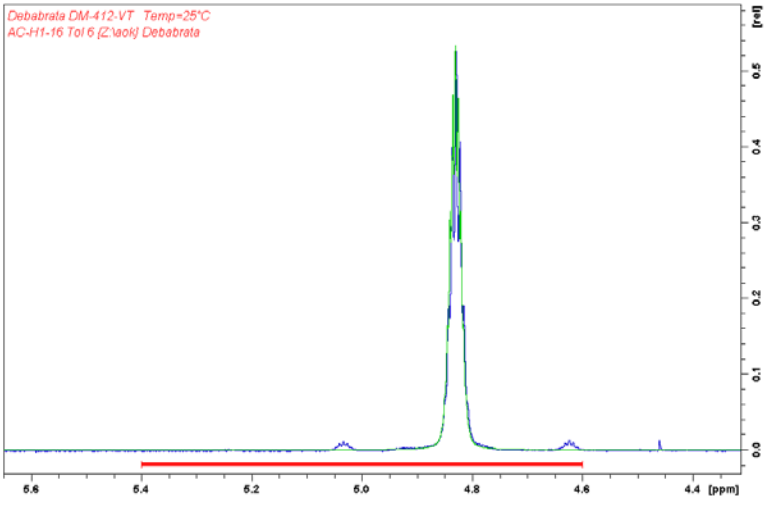

Figure S26. Experimental (blue) and simulated (green) ^{1}H NMR spectra of **6** for line shape analysis. The red bar marks the refined area.

An Eyring plot derived from the above analysis provides the activation parameters as $\Delta H^{\ddagger}$ = 9.7±0.8 kcal mol^{-1} and $\Delta S^{\ddagger}$ = –8.0±0.4 cal mol^{-1} K^{-1} that lead to $\Delta G^{\ddagger}_{253K}$ = 11.7±0.9 kcal mol^{-1} at the coalescence temperature 253 K.

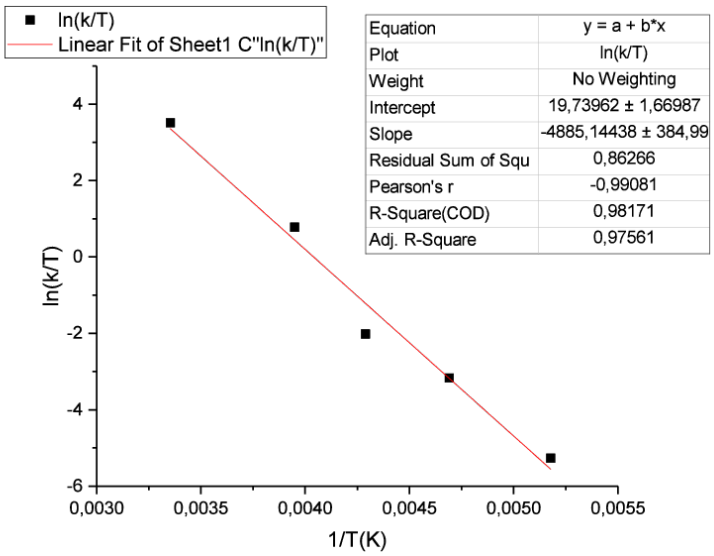

Figure S27. Eyring plot for the simulated exchange rates.

4. X-ray crystallography.

Single-crystal X-ray diffraction measurements of **1**, **2**, **3**, **4** and **5** were performed on a Bruker AXS diffractometer equipped with an Incoatec microsource and an APEX area detector using MoKα radiation (λ = 0.71073 Å), multilayer optics and ω-scans. Temperature control was achieved with an Oxford cryostream 700. The SMART program was used for data collection and unit cell determination; processing of the raw data frame was performed using SAINT+,[S2] multi scan absorption corrections were applied with SADABS.[S3] The structures were solved by direct methods (SIR-92).[S4] **1** shows crystallographic inversion symmetry for the molecule. Compound **2** shows crystallographic C_2 symmetry, atom Si1 is located on the axis of rotation. The CH_2 carbon atoms of the Me_3TACD ligands in **1** (C1 – C8) are disordered. The disorder could be modeled with split positions. The CH_2 carbon atoms of the Me_3TACD ligand in **2** as well as the amido nitrogen atom N2 and the CH_3 carbon atom C6 are disordered. The disorder was modeled with split positions. The refinements were performed against F^2 with the program SHELXL-2013 using all reflections.[S5] Hydrogen atoms were included as riding on calculated positions with U_{iso}(H) = 1.2U_{eq}(C) or 1.5$U_{eq.}$(non-H), except for the atoms bound

to silicon (H1 and H2 in **2**, H2, H3 and H4 in **3** as well as H2 in **4**, H1 and H2 in **5**). These atoms were localized in difference Fourier maps and refined in their position with isotropic displacement parameters $U_{iso}(H) = 1.2U_{eq}(Si)$. All non-hydrogen atoms were refined anisotropically. Refinement results are given in Table S1. Graphical representations were performed with the program DIAMOND.[S6] CCDC-1537652 (**1**), -1537653 (**2**), -1537654 (**3**), -1537655 (**4**), -1537656 (**5**) contain the supplementary crystallographic data for this paper. These data can be obtained free of charge from the Crystallographic Data Centre via www.ccdc.cam.ac.uk/data_request/cif.

Table S1. Crystal data and structure refinement.

	1	**2**	**3**	**4**	**5**
chemical formula	$C_{34}H_{86}N_{10}Si_4Sr_2$	$C_{19}H_{54}N_6Si_4Sr$	$C_{19}H_{52}N_6Si_4Sr$	$C_{21}H_{56}N_6Si_4Sr$	$C_{15}H_{39}N_5MgSi_2$
fw ($g \cdot mol^{-1}$)	922.72	566.66	564.64	592.69	370.00
space group	$P2_1/n$	$C2/c$	$P\bar{1}$	$P2_12_12_1$	$Pbca$
crystal size (mm)	0.17×0.18×0.38	0.32×0.38×0.42	0.17×0.33×0.34	0.13×0.16×0.27	0.21×0.45×0.49
unit cell parameters					
a (Å)	9.3831(12)	21.541(2)	9.2006(18)	10.6835(18)	17.331(15)
b (Å)	26.657(3)	10.4100(11)	9.5438(9)	17.274(3)	13.273(12)
c (Å)	9.8491(12)	16.409(5)	19.2910(18)	17.745(3)	18.878(18)
α (°)			81.0103(14)		
β (°)	100.519(2)	121.6531(15)	87.999(15)		
γ (°)			68.1159(14)		
V ($Å^3$)	2422.1(5)	3132.2(11)	1552.4(4)	3274.8(10)	4343(7)
Z	2	4	2	4	8
T (K)	100(2)	100(2)	100(2)	100(2)	110(2)
μ(Mo K_α) (mm^{-1})	2.335	1.891	1.908	1.812	0.199
reflns	25518	21371	19280	10065	24014
independent reflns ($R_{int.}$)	6076 (0.0784)	3922 (0.0444)	6526 (0.0460)	6158 (0.0603)	4227 (0.0582)
observed reflns	4711	3311	5726	4488	3505
parameters	315	202	291	305	221
goodness of	1.010	1.033	0.943	0.928	1.040

fit on F^2					
final R indices					
$R1$, $wR2$ $[I \geq 2\sigma(I)]$	0.0403, 0.0827	0.0290, 0.0686	0.0322, 0.0764	0.0572, 0.1131	0.0394, 0.0962
$R1$, $wR2$ (all data)	0.0608, 0.0898	0.0386, 0.0718	0.0392, 0.0796	0.0894, 0.1262	0.0509, 0.1046

5. References.

S1 Bruker, TopSpin 3.2, Bruker BioSpin, Billerica, Massachusetts, 2013.

S2 Bruker, SAINT-Plus, Bruker AXS Inc., Madison, Wisconsin, USA, 1999.

S3 Bruker, SADABS, Bruker AXS Inc. Madison, Wisconsion, USA, 2004.

S4 A. Altomare, G. Cascarano, C. Giacovazzo and A Guagliardi, A. *J. Appl. Crystallogr*. 1993, **26**, 343-350.

S5 G. M. Sheldrick, *Acta Crystallogr. Sect. A*, 2008, **64**, 112–122.

S6 K. Brandenburg, DIAMOND, Crystal Impact GbR, Bonn, Germany, 2017.